IOP Publishing Journal of Physics D: Applied Physics

J. Phys. D: Appl. Phys. **48** (2015) 355101 (10pp) doi:10.1088/0022-3727/48/35/355101

Low temperature characteristic of ITO/SiO_x/c-Si heterojunction solar cell

H W Du[1], J Yang[1], Y Li[1], M Gao[1], S M Chen[1], Z S Yu[3], F Xu[1] and Z Q Ma[1,2]

[1] SHU-SolarE R&D Lab, Department of Physics, SHU-SolarE R&D Lab, Shanghai University, Shanghai 200444, People's Republic of China
[2] Instrumental Analysis & Research Center, Shanghai University, Shanghai 200444, People's Republic of China
[3] School of Electrical, Computer and Energy Engineering, Arizona State University, Tempe, AZ 85287-5706, USA

E-mail: zqma@shu.edu.cn

Received 20 March 2015, revised 18 June 2015
Accepted for publication 25 June 2015
Published 5 August 2015

Abstract

Based on the temperature-dependent measurements and the numerical calculation, the temperature response of the photovoltaic parameters for a ITO/SiO_x/c-Si heterojunction solar cell have been investigated in the ascending sorting of 10–300 K. Under unique energy concentrated photon irradiation with the wavelength of 405 nm and power density of 667 mW cm^{-2}, it was found that the short-circuit current (I_{SC}) was nonlinearly increased and the open-circuit voltage (V_{OC}) decreased with temperature. The good passivation of the ITO/c-Si interface by a concomitant SiO_x buffer layer leads to the rare recombination of carriers in the intermediate region. The inversion layer model indicated that the band gap of c-silicon was narrowed and the Fermi level of *n*-type silicon (E_F^n) tended to that of the intrinsic Fermi level (E_F^i) (in the middle of band gap) with the increase of the temperature, which lessened the built-in voltage (V_D) and thus the V_{OC}. However, the reduction by 90% of V_{OC} is attributed to the shift of E_F^n in c-silicon rather than the energy band narrowing. Through the analysis of the current–voltage relationship and the data fitting, we infer that the series resistance (R_s) is not responsible for the increase of I_{SC}, but the absorption coefficient and the depletion-width of c-silicon are the causes of the enhancing I_{SC}. Mostly, the interaction of the photon-generated excess 'cold hole' and the acoustic phonon in n-Si would influence the variation of I_{ph} or I_{SC} with temperature.

Keywords: ITO/SiO_x/c-Si, short-circuit current, open-circuit voltage, temperature response

(Some figures may appear in colour only in the online journal)

1. Introduction

So far, crystalline silicon solar cells are dominant in the photovoltaic field due to their high efficiency, low selling price and process maturity. However, the energy intensive processes, such as metallization, are a barrier for further reducing the costs of electricity, which restrict the mass application of solar cells [1, 2]. Amorphous silicon based technology such as heterojunction intrinsic thin film (HIT) solar cells reduces the material consumption and processing temperature, but more complicated process steps are required to compensate the efficiency loss induced by crystal defects, which impairs its cost advantages [3, 4]. A solar cell with fewer bulk defects, high stability, simple technology and low energy cost is the ultimate goal. Consequently, one kind of semiconductor-insulator-semiconductor (SIS) heterojunction solar cell composed of transparent-conductive-oxides (TCO), silicon oxide (SiO_x) and crystalline silicon (c-Si) has been resurrected in recent research [5–7]. Among the various TCO films, In_2O_3 : SnO_2 (ITO) film is the most well-investigated and widely applied as a window layer in thin film optoelectronic devices, with resistivity as low as 1×10^{-4} Ω cm and transmittance as high as 90% at the wavelength of 550 nm [8]. To form a SIS solar cell, one of the most used methods is to directly deposit the TCO

 © 2015 IOP Publishing Ltd Printed in the UK

films on silicon substrates at a low temperature (<300 °C), eliminating the high temperature firing process. Moreover, the stability of SIS solar cells can be compared with a crystalline silicon cell as the photovoltaic effect happens in the bulk silicon. In addition, the advantages of TCO films in the structure are that they not only act as a high transparent and conductive window layer, but also assist as a semiconductor and quasi-metal layer of built-in field [9].

During deposition processing of the ITO film, the ultra-thin interfacial layer SiO_x can be naturally formed and potentially used to passivate the dangling bonds at the interface, reducing the interface recombination which has great negative influences on device performance [10–13]. Nevertheless, an energy barrier at the interface is usually subjoined by SiO_x, therefore the electrons or holes have to flow through the barrier by tunneling [14]. The SiO_x layer should be sufficiently thin (1–2 nm) so that the tunneling probability can be increased, and its quality should be good so that the interface states are reduced to a low level [13, 15]. Considering the ground application of solar cells, the interest temperature scope for regarding the stability of a solar cell is from −80 to 80 °C in previous research [16–18]. Actually, the device performance of a SIS solar cell is restricted by the tunneling characteristic and the interface recombination, both of their behaviors at low temperature (<100 K) are completely different from that at room temperature [19–21]. At a high temperature, the carriers are activated to a higher energy to form thermal-related current and lots of phonons participate in the recombination. Therefore, to perform the current–voltage (*I–V*) trait at low temperature on SIS solar cells, one is able to analyze the tunneling and the recombination mechanism, and then it is possible to provide further guidance for the optimization of device performance.

Therefore, with the goal of studying low temperature effect of a PV device, we choose the SIS structure for the investigation of its temperature response, as well as the exploration of its behavior of carrier transport and recombination in the device system. Combining the *I–V* measurement with the reduced characteristic formula, we not only show the varying rule of the device, but also the essential relationship of the physics parameters by the numerical fitting.

2. Experimental details

N-type silicon (n-Si) substrates with dopant phosphorous concentration of 1.5×10^{15} cm^{-3} were used in the experiment and were cleaned using standard RCA cleaning process, followed by 5% HF dip to remove native SiO_x. 250 nm thick ITO film was deposited directly on the n-Si substrate by radio frequency (RF) magnetron sputtering in Ar atmosphere. The power is 100 W, the substrate temperature is 250 °C, the base pressure is 2×10^{-4} Pa and the work pressure is 1.0 Pa. The ITO target is composed of 90 wt% In_2O_3 and 10 wt% SnO_2. The O atoms of ITO may possibly diffuse into the surface region of Si substrate and combine with Si to form Si–O bond, thereby an ultra-thin SiO_x layer was spontaneously formed between ITO and c-silicon substrate, being happy to bring about an effective passivation of the ITO/c-Si interface during the sputtering process [6]. Ag (100 nm)/Al (1 μm) grid electrode was evaporated on the front side and the 2 μm Al electrode was evaporated on the back side. The active area of the cell is 0.72 cm^2.

Table 1. The composition, transmission and electrical properties of ITO film.

	Parameters
Chemical composition	In:O:Sn = 45.8:51.0:3.2
Average transmission	350–800 nm: 90%
Electrical properties	n: 3.8×10^{20} cm^{-3};
	μ_n: 39.4 cm^2 $V^{-1} \cdot S^{-1}$; ρ: 4.2×10^{-4} Ω cm

The chemical stoichiometric composition of ITO films were attained by using ESCALAB 250Xi x-ray photoelectron spectrometer (XPS) with the Al kα (1486.6 eV) source, and the Argon ion milling was used for the depth etching to obtain the chemical states of n-Si surface at the intermediate region of ITO/c-Si. The minority lifetimes of n-Si were measured by using a μ-PCD device (Semilab WCT-2000). A 200 ns laser pulse at 904 nm was used for exciting photon-generated carriers. The transmission spectra and the electronic properties of ITO films were measured by TU1901 UV-VIS spectrophotometer and Crosstech HMS300 Hall Instrument, respectively. Two modes were separately established for measuring specific *I–V* curves under standard conditions and then the PV optoelectronic parameters at low temperature. Firstly, the *I–V* curve was obtained by using a Keithley 2400 under AM1.5G illumination, and also the capacitance-voltage (*C–V*) curve was carried out by using Agilent E4980A under 1 MHz, at 25 °C. The build-in potential was extracted from the extrapolation of $1/C^2$ dependent on the applied voltage V to zero. Secondly, the *I–V* curves under the low multiple concentrated laser illumination in the range of 10–300 K were measured by using Agilent 4155C. Restricted by our apparatus, in the low temperature measurement, *I–V* was obtained under 405 nm laser-irradiation, with a power of 20 mW and a spot size of 0.03 cm^2.

3. Results and discussion

3.1. ITO materials & interface configuration

In order to evaluate the quality of ITO films deposited on n-Si substrate by magnetron sputtering, the XPS and Hall measurements were used to analyze its composition, transmission and electronic properties, which are listed in table 1. The n, μ_n and ρ in table 1 are the carrier concentration, the mobility of the electron and the resistivity, respectively. The high average transmission of 90% and the low resistivity of 4.2×10^{-4} Ω cm implicitly indicate that the low temperature deposition process has the capacity to prepare high quality ITO films for the SIS solar cells.

There are three peaks with the binding energy of 99.1, 99.7 and 102.9 eV in the Si 2p spectrum in ITO/c-Si interfacial region, shown in figure 1. The peaks at 99.1 and 99.7 eV are related to the spin–orbit doublet of elemental Si, denoted as $2p_{3/2}$ and $2p_{1/2}$ electronic levels [22]. The band at 102.9 eV is

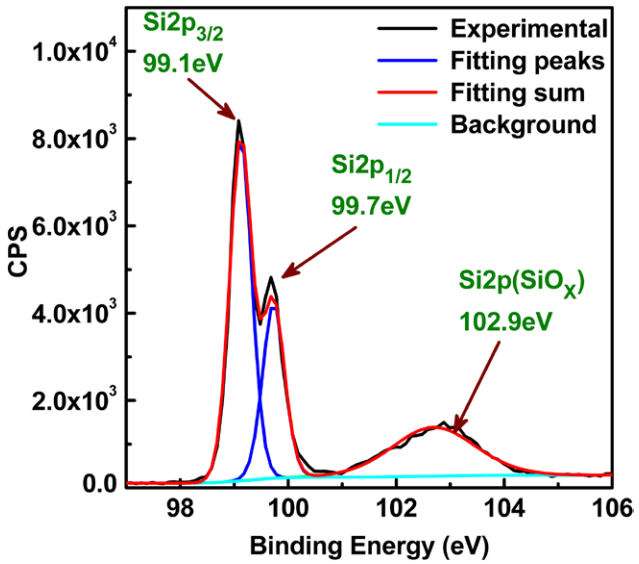

Figure 1. XPS of Si 2p in ITO/c-Si interfacial region. The XPS at the interface is obtained by Argon ion milling etching.

apparently to be the direct evidence for the existence of SiO_x at the interface region. According to Si 2p the intensity ratio of the SiO_x layer and substrate n-Si, the thickness is estimated to be about 1.5 nm [23]. In our previous study, the thickness of SiO_x measured by the cross-sectional transmission electron microscope (TEM) is 1.8 nm which is close to the estimated value [6]. As the silicon substrate has been dipped by 5% HF to remove the native SiO_x, there is no doubt that the SiO_x is generated during the sputtering process. The O elements to form SiO_x are most likely from ITO material, because the base pressure of the deposition chamber is 2×10^{-4} Pa, there are barely residual oxygen atoms.

To assess the passivated effect of SiO_x layer, the minority carrier lifetimes of silicon without and with SiO_x layer are measured, which are shown in figures 2(a) and (b), respectively. After being passivated, the average minority carrier lifetime of silicon is increased from 2 to 35 μs, indicating that the SiO_x at ITO/c-Si interface provides a beneficial effect on device performance owing to its function to passivate the interface states to enhance the open-circuit voltage (V_{OC}) and fill factor (FF) as well. Although better passivation would be provided with the thicker SiO_x, the probability of carrier tunneling would be decreased, which is harmful to the device performance. The thickness of 1.5 nm of SiO_x layer is a balanced result of the passivation and current.

3.2. Device performance

The photovoltaic feature (V_{OC}) under one-sun AM1.5G illumination and the derived built-in voltage ($V_{D\text{-}CV}$) from $1/C^2 - V$ curve at room temperature of SIS solar cell has been carried out in figures 3(a) and (b), respectively. Based on the architecture of the device with the heterojunction electronic structure for electron and holes in the transportation, the tunneling-recombination model results in a set of optoelectronic parameters, i.e. the open-circuit voltage V_{OC} of 0.51 V, short-circuit current density J_{SC} of 24.3 mA cm^{-2}, and filled factor FF of 71.1%, which leads to a power conversion efficiency (Eff) of 8.8%. For silicon materials, the short-circuit current density (J_{SC}) is affected by surface reflection and absorption; V_{OC} depends on the saturation current (J_0) of the solar cell and the light-generated current (J_{SC}). While the J_{SC} typically has a small variation, the key effect is the saturation current, since this may vary by orders of magnitude. The saturation current, J_0 depends on recombination in the solar cell. V_{OC} and FF are then the measure of the amount of recombination in the device. Also V_{OC} is limited by actual built-in voltage (V_D) and the band gap (E_g) as well. Both J_{SC} and V_{OC} determine the efficiency (Eff).

Thus, in figure 3(a), the relatively high FF indicates a low recombination both in bulk and at the interface, which also suggests that even though we eliminated oxidation process, the ITO/c-Si interface passivation is still good with the induced SiO_x. Figure 3(b) shows the $1/C^2 - V$ curve of SIS solar cells. The value of V_{DCV} is only 0.57 V which limits the V_{OC}. On the other side, there is no anti-reflection coating on the surface, so that the optical loss is quite high which results in the lower J_{SC}. Therefore, further optimization should be focused on the improvement of V_D and reducing optical loss so as to increase the efficiency.

In order to understand the electronic structure of the device system, we figured out a draft of the energy band shown in figure 4, additionally, the estimations of the values based on the semiconductor parameters, such as electron affinity, work function, band gap and Fermi levels, are also denoted in figure 4. As ITO is an n-type heavily doped degenerate semiconductor, and this trait induces that the built-in potential is almost located in the silicon substrate. Similar to the HIT-like solar cell, the space charged region consists of the depletion region and surface inversion layer emitter inside n-Si, in which a high electric field in the surface layer of silicon substrate is induced [24, 25]. Significantly, the heavily doped degenerate ITO film, with its high quality of semiconductor and/or quasi-metal properties, is helpful to the formation of the inversion layer emitter within the hetero-interface. Referring to the experimental measurement and theoretical estimation, the value of the built-in voltage ($V_{D\text{-}FL}$) derived by the difference of Fermi levels between silicon and ITO is about 0.68 V. $V_{D\text{-}FL}$ represents the maximum value of V_D in the device. The effects of the surface potential and the recombination loss in this device are responsible for $V_{D\text{-}FL} > V_{D\text{-}CV} > V_{OC}$.

3.3. Temperature response

The complete temperature response of the SIS device performance under concentrated photons irradiation is shown in figure 5, where the Max(IV) means the maximum conversion power point in the temperature dependent I–V curves and represents the Eff. The temperature dependences of Max(IV), FF, I_{SC} and V_{OC} are illustrated by figures 5(a)–(d), respectively. As the temperature increases from 10 to 300 K, I_{SC} is enhanced from 2.26 to 3.84 mA cm^{-2}; whereas V_{OC} drops from 0.74 down to 0.46 V; both of FF and Max(IV) fluctuates as the temperature changes. Hereon FF and Max(IV) in general are insensitive to the temperature. From the variation

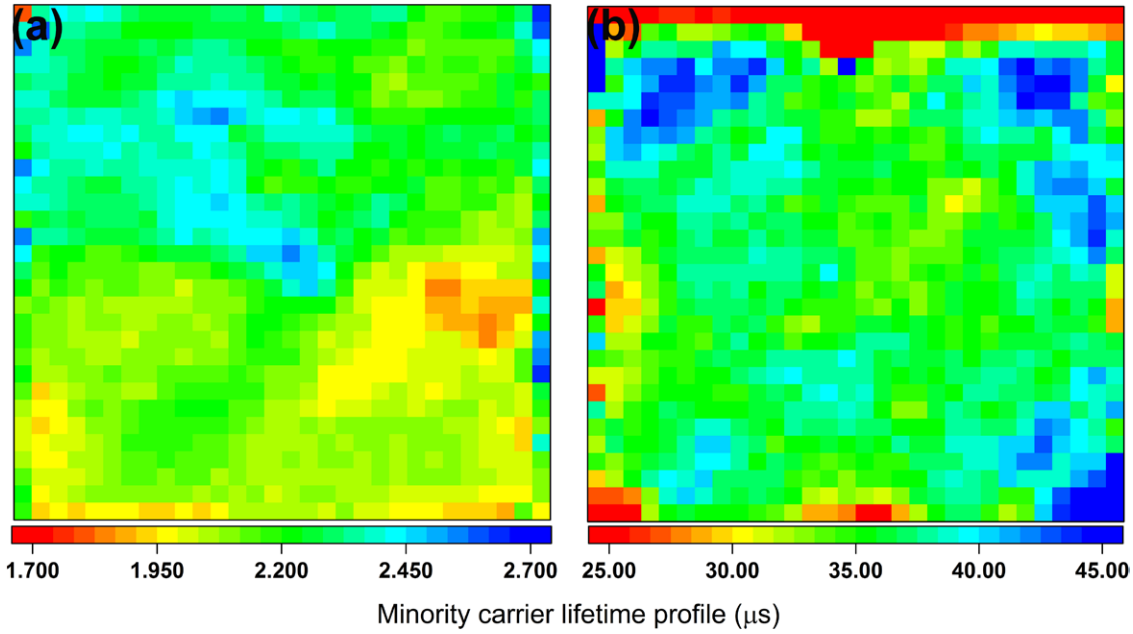

Figure 2. The minority carrier lifetime: (a) bare silicon and (b) silicon with SiO_x.

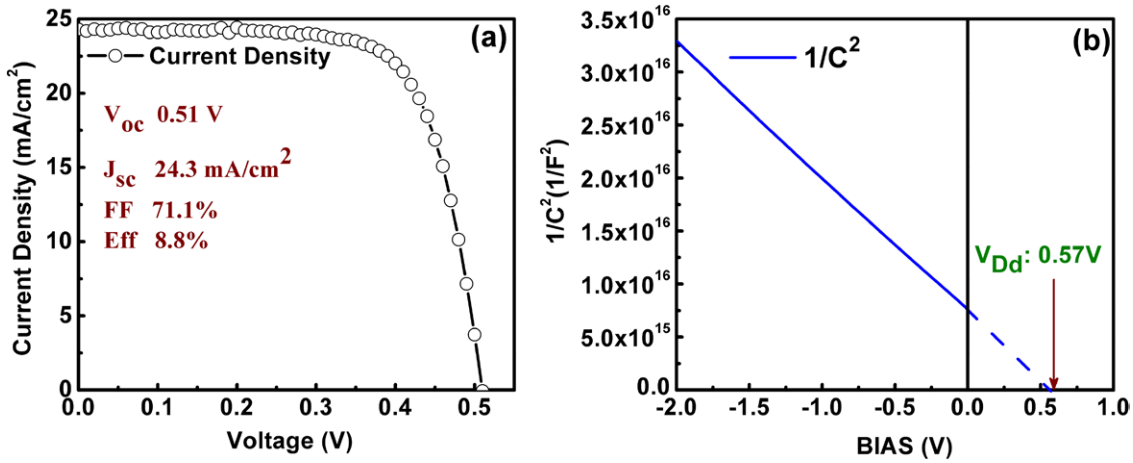

Figure 3. (a) *I–V* curve under one-sun AM1.5G illumination and (b) $1/C^2 - V$ curve at for SIS solar cell at room temperature.

of V_{OC} and I_{SC} with the temperature, we can conclude that the unequal compensated causes exist in the process. Thus, the conversion efficiency is almost invariable with the temperature. The stable *FF* indicates that the carrier recombination in this device is insensitive to the temperature as well.

Actually, the above results and discussion also demonstrate the importance of the ideality factor (n) of the SIS PV device, as n is a measure of the junction quality and the type of recombination in a diode as well as a solar cell. For the simple recombination mechanisms discussed in the elsewhere, the n-factor has a value of 1. However, some recombination mechanisms, particularly if they are large, may introduce recombination mechanisms of 2. A high n-value not only degrades the *FF*, but since it will also usually signal high recombination, it gives low open-circuit voltages. In our case, it is more than 1 but lower than 2. Then only *FF* is able to objectively reflect the carrier recombination in the device. However, the experimental results indicate that the interface recombination of carriers in the SIS device is independent of the temperature.

Besides the *FF* factor, the low temperature-correlated variations of V_{OC} and J_{SC}, being applied to the carrier recombination mechanisms, are evaluated in the following sections.

3.3.1. Open-circuit voltage. It is well-known that the V_{OC} is basically enforced by two causes: one is electron–hole recombination; and another is potential height V_D in a solar cell. The larger V_D is in the device, the larger V_{OC} obtains in the device; and the larger carrier recombination is, the smaller V_{OC} becomes, as well. Thus, combing the experimental data and the previous issued formula, we try to extract the impact of the recombination on V_{OC} through the *I–V* relationship of the diode, at the open circuit condition. The ideal diode's *I–V* relationship is expressed as following [26]:

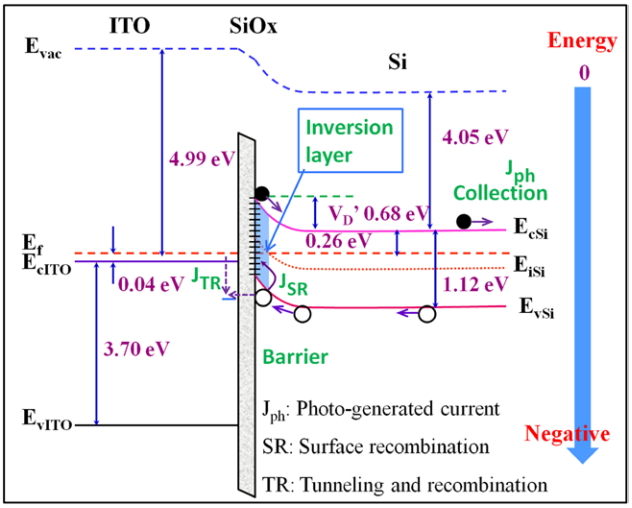

Figure 4. The energy band diagram and carriers transportation under lamination of SIS solar cell.

$$0 = I_{ph} - I_0\left[\exp\left(\frac{V_{OC}}{k_0T/q}\right) - 1\right] - \frac{V_{OC}}{R_{sh}} \quad (1)$$

where I_{ph} is the photon-generated current, I_0 is the saturation current, k_0 is the Boltzmann constant, T is the absolute temperature, q is the electron charge and R_{sh} is the shunt resistance.

The values of parameters R_{sh} and I_0 in equation (1) may be impacted by the electron–hole recombination as they are correlated together in the formula. In this work, the method to extract parameters of diode from *I–V* curves is same as reference [26]. The shunt resistance (R_{sh}) is due to the leakage currents (I_{sh}) of the diodes. The shunt resistance includes two parts: the bulk and surface leakage current. The leakage current gives rise to equations similar in form to the recombination current obtained with the recombination model. The bulk leakage current is increased with the dislocated density, which is similar to the bulk recombination current that is increased with bulk defect density. And the surface states provide the leakage channels to increase the surface leakage current, which is also similar to the surface recombination current. Thus, the change trends of recombination can be reflected by R_{sh}. It is found that the value of R_{sh} is almost invariable over the whole temperature range, as shown in figure 6(a). Thus, the carrier recombination in this device independent of the temperature is reconfirmed by R_{sh}. From the measurements in figure 6(a), we saw a big measure of R_{sh} in the order of 10^4 Ω, which also proved that the recombination is as little as in SIS device. On the other side, the value of R_{sh} is large enough to ignore its effect on the device performance. Then the V_{OC} of SIS device can be approximately expressed as:

$$V_{OC} = \frac{nk_0T}{q}\ln\left(\frac{I_{ph}}{I_0}\right) = \frac{nk_0T}{q}\ln(I_{ph}) + \left(-\ln(I_0) * \frac{nk_0T}{q}\right) \quad (2)$$

where $1 < n < 2$.

In the previous studies, it has demonstrated that an increase of I_0 with temperature would cause a linear increase of V_{OC} in the range of −80 to 80 °C [27–29]. However, in our investigation, the second term in equation (2) grows with temperature

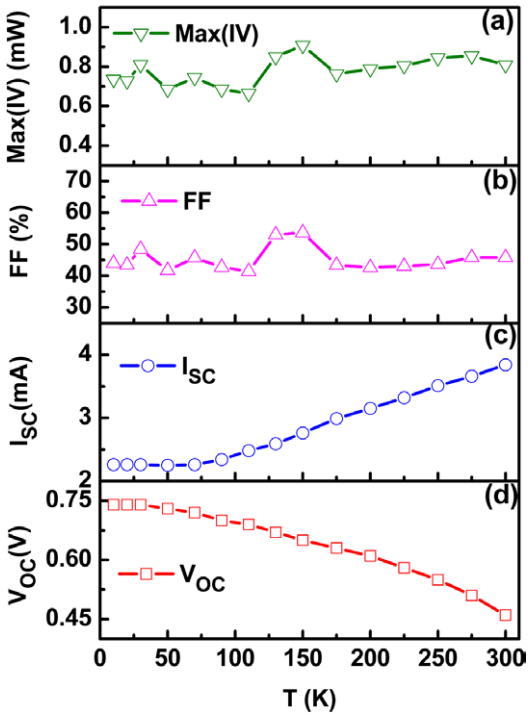

Figure 5. The temperature dependence of (a) Max(*IV*), (b) *FF*, (c) I_{SC} and (d) V_{OC}.

as shown in figure 6(b). Although the product factor $-\ln(I_0)$ decreases as the temperature increases (not shown here), the k_0T/q variation with the temperature results in the improvement of $-\ln(I_0)$ k_0T/q. From the view of point on I_0, the temperature has a positive effect on V_{OC} rather than the negative influence. Therefore, for the SIS device, the carrier recombination might not be the main reason accounting for the drop of V_{OC} when the temperature rises. On the other hand, in our experiment, the measured V_{OC} at 10 K is as high as 0.74 V, which is even larger than the value of $V_{D\text{-}FL}$ = 0.68 V at 300 K. This also indicates that the V_D increases as the temperature decreases, leading to an increase of V_{OC} and the potential difference being a main reason. It is hard to place an accurate amount on V_D. In this work, we suppose that the effects of temperature on both V_D and $V_{D\text{-}FL}$ are same.

In the above mentioned, the $V_{D\text{-}FL}$ of SIS device is determined by the difference of Fermi levels between ITO and silicon, its formal expression is given by:

$$V_{DFL} = \frac{E_{fSi} - E_{fITO}}{q} \quad (3)$$

where, E_{fSi} and E_{fITO} are the positions of Fermi levels of Si and ITO materials, respectively. However, ITO as a degenerate semiconductor, its Fermi level is already above the conduction band even at room temperature, so it barely changes with temperature as elucidated in the literature [30]. Thus, the change of V_{DFL} is determined by E_{fSi}. Consequently, the variable $\Delta V_{D\text{-}FL}(T)$ is dependent on the temperature as follows:

$$\Delta V_D(T) = \Delta V_{DFL}(T)\begin{cases} = V_D(T) - V_D(10\,\text{K}) & \text{or} \\ = \Delta E_{fSi}(T)/q & \text{or} \\ = [\Delta E_{cSi}(T) - \Delta(E_{cSi}(T) - E_{fSi}(T))]/q \end{cases} \quad (4)$$

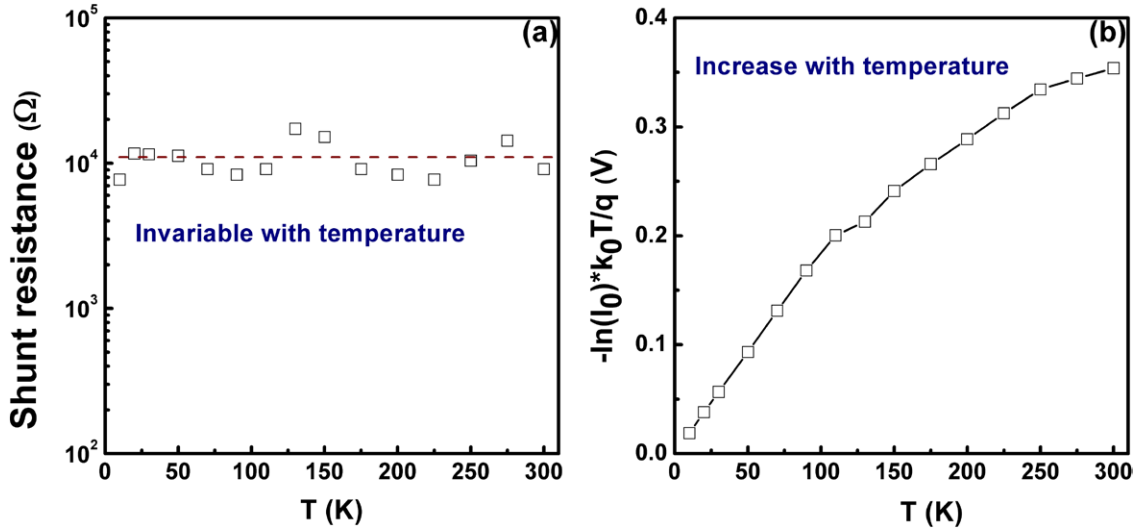

Figure 6. The temperature dependence of (a) R_{sh} and (b) $-\ln(I_0)*k_0T/q$.

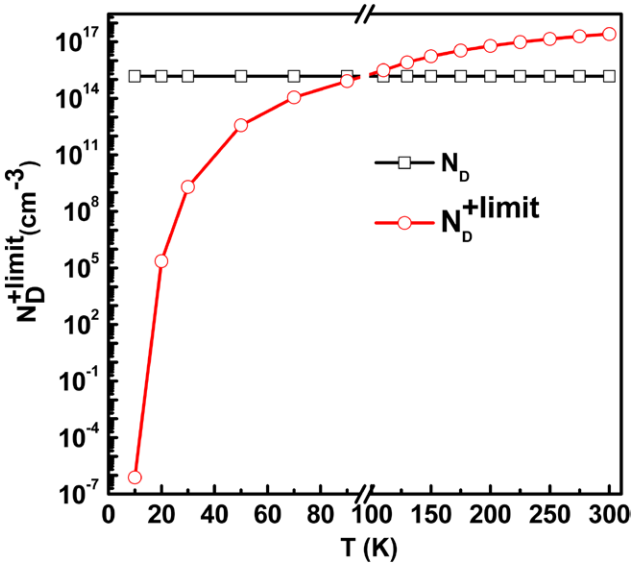

Figure 7. The relationship of N_D^{+limit} and temperature.

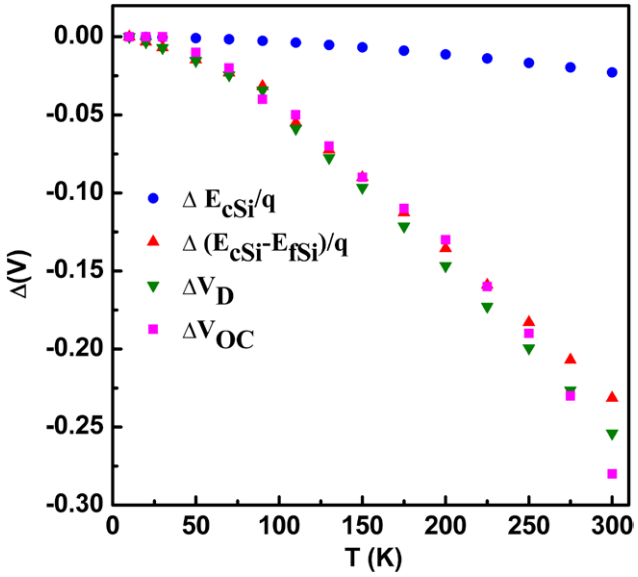

Figure 8. The temperature dependence of $\Delta E_{fSi}/q$, $\Delta(E_{cSi} - E_{fSi})/q$, ΔV_D and ΔV_{OC}.

From equation (4), there are two kind effects of temperature acting on E_{fSi}: one is to vary the band gap through changing the position of conduction band edge (E_{cSi}); and the other is to vary the ionized level by means of changing the relative position of Fermi level in band gap ($E_{cSi} - E_{fSi}$).

The relation of a semiconductor band gap dependent on the temperature is ascribed by [31]:

$$E_g(T) = E_g(0) - \frac{\alpha T^2}{\beta + T} \tag{5}$$

where $E_g(0)$ is the band gap at 0 K; α and β are the corresponding thermal coefficients. For silicon, values of $E_{gSi}(0)$, α_{Si} and β_{Si} are 1.170 eV, 4.73×10^{-4} eV K^{-1} and 636 K, respectively. In a rough approximation, the assumption for a change of E_{gSi} contrasted to the half change of E_{cSi} has been considered.

Therein, the value of $(E_{cSi} - E_{fSi})$ in *N*-type semiconductor is determined by the doping concentration and the temperature, and its expression is given by:

$$\begin{cases} E_c - E_f = -\dfrac{\Delta E_D}{2} - \left(\dfrac{k_0T}{2}\right)\ln\left(\dfrac{N_D}{2N_c}\right), \text{weak ionization} \\ E_c - E_f = -k_0T\ln\left(\dfrac{N_D}{N_c}\right), \text{strong ionization} \end{cases} \tag{6}$$

where ΔE_D is the dopant ionization energy, N_D the donor concentration and N_c the effective state density in the conduction band. For phosphorous elements in Si, ΔE_D is in a small value of 0.044 eV.

In the thermodynamic equilibrium, presuming the ionized dopants of 90% are strong ionization, the limit of ionization concentration in terms of temperature can be expressed as [32]:

$$N_D^{+limit} = \left(\frac{D\_N_c}{2}\right)\exp\left(-\frac{\Delta E_D}{k_0T}\right)$$
$$N_c = 2\frac{(2\pi m_n^* k_0T)^{3/2}}{h^3} \tag{7}$$

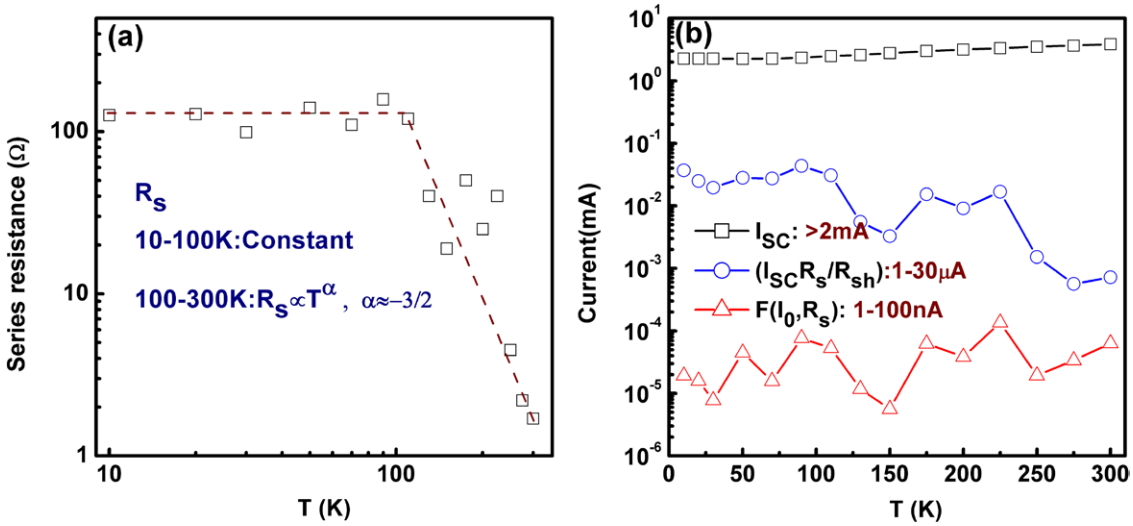

Figure 9. (a) the relationship of R_s and temperature, and (b) the effects of temperature on $F(I_0, R_s)$, I_{SC} R_s/R_{sh} and I_{SC}, respectively.

where, D_- is the unionized fraction, with a value of 0.1. m_n^* is the effective mass of electron, and h is the Planck constant. The relationship of $N_D^{+\text{limit}}$ with the temperature is plotted in figure 7. It is shown that the cross point between the strong and weak ionization is near 100 K.

Furthermore, the temperature dependence of $\Delta E_{fSi}/q$, $\Delta(E_{cSi} - E_{fSi})/q$, ΔV_D and ΔV_{OC}, are calculated with equations (1)–(3), respectively. The results are plotted in figure 8. Here the $\Delta E_{fSi}/q$, $\Delta(E_{cSi} - E_{fSi})/q$, ΔV_D and ΔV_{OC} are defined as the change of the energy band gap, difference between the conduction band edge and Fermi level, potential barrier and open-circuit voltage from c-Si side, respectively. The band gap E_{gSi} turns narrow and the Fermi level E_{fSi}, at the same time, moves downward to the intrinsic level correspondingly, as the temperature increases. During the process, the value of $(E_{cSi} - E_{fSi})$ gets larger with the temperature. Thus the V_{OC} drops with the temperature. Obviously, the downward trends of ΔV_D and ΔV_{OC} are basically identical, which confirms that the change of V_D and V_{OC} is closely correlated within the scope of the temperature. The measure of E_{cSi} decreases by 23 meV and the $(E_{cSi} - E_{fSi})$ decreases by 232 meV, in which the V_D is finally reduced by 0.26 V, accompanying the temperature from 10 to 300 K. According to the experimental data and estimation, we can claim that the shift of E_{fSi} in the band gap devotes about 90% for the reduction of V_{OC}, while the other 10% contribution may be due to the energy band gap narrowing. The lessened value of V_D is less than that of the V_{OC} reduction, which may be caused by the carrier recombination in the intermediate region of ITO/SiO_x/n-Si system.

3.3.2. Short-circuit current. The change of the short-circuit current (I_{SC}) with the temperature is another important subject in our investigation of the SIS solar cells. From the knowledge of a solar cell, the I_{SC} is mainly affected by the absorption (related to photon-generated current) and the parasitic resistance in the heterojunction materials, which has been summarized in the formula [26]:

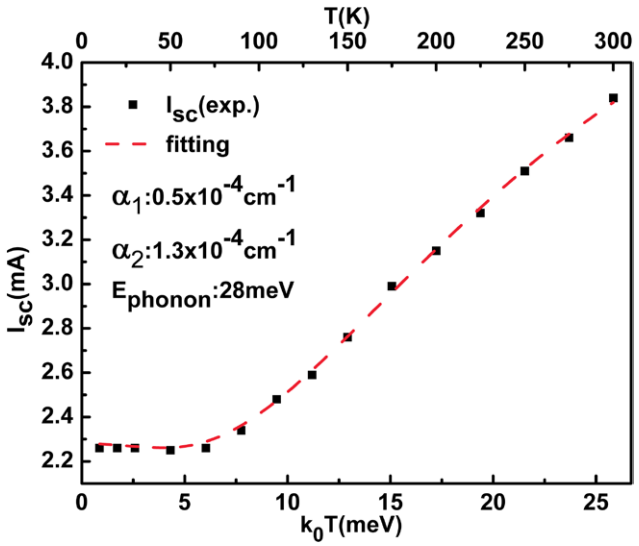

Figure 10. The results of fitting I_{SC} to equation (15).

$$I_{SC} = I_{ph} - I_0\left[\exp\left(\frac{I_{SC}R_s}{nk_0T/q}\right) - 1\right] - \frac{I_{SC}R_s}{R_{sh}} \tag{8}$$

where, the R_s is the series resistance. Figure 9(a) shows the temperature dependent R_s, which does not change below 100 K, but exponentially decreases from 100 to 300 K, and it can be fitted to the power of −3/2. Additionally, as the ITO films can be used as a quasi-metal material in the present because of its high electron concentration and low resistivity, the value of R_s in the SIS solar cell could be reasonably substituted by the bulk resistance of silicon. Thus, it is given by the formula [32]:

$$R_s \approx \frac{1}{A_s}\frac{1}{n_0 q \mu_n} \tag{9}$$

where A_s is the sample area; μ_n is the mobility of the electron; n_o is the electron concentration. Below the 100 K, the dopants are not fully ionized (refer to section 3.3.1), and the

Table 2. The specific values of those physical parameters for fitting.

Parameters	N	ε (F/m)	q (C)	k_0 (J/K)	V_D (V)
Value	4.08×10^{16}	1.05×10^{-10}	1.602×10^{-19}	1.38×10^{-23}	0.68–0.93

acoustic phonon scattering is the main scattering mechanism at the low temperature scope [32]. As the temperature rises, n_o increases as more dopants are ionized, whereas μ_n drops due to the increase of phonon scattering, thus these two effects tradeoff each other, so that the R_s does not change. Above 100 K, the dopants are fully ionized and n almost keeps constant, and the main scattering mechanism is from ionized impurity scattering. Under this condition, μ_n increases in the power of 1.5 with the temperature [32]. As a result, the R_s exponentially decreases with the temperature.

Letting the second item of equation (8) be fixed as $F(I_0, R_s)$, because it is variable as small as 1–70 nA in the range of 10–300 K, the values of first and third items of the right hand side of equation (8) are estimated in order to evaluate their effects on I_{SC}. Figure 9(b) shows the effects of temperature on $F(I_0, R_s)$, $I_{SC}R_s/R_{sh}$ and I_{SC}. The values of $F(I_0, R_s)$ and $I_{SC}R_s/R_{sh}$ are far smaller than I_{SC}, which illustrates that the changes of R_s is not the main reason resulting in the increase of I_{SC} as temperature rises. In consequence, the varation of I_{SC} is controlled by I_{ph}. Neglecting the infinitesimals, we can rewrite the equation (8) as:

$$I_{SC} \approx I_{ph} \tag{10}$$

The Green has pointed out that the I_{ph} slightly increased with temperature, because the decrease of the band gap enlarges the absorption spectrum. However, in this case the I_{SC} increases by 70%, and the temperature does not change the absorption spectrum because of the single excitation sources. This suggests that the collective way of photo-generated carriers for this device is different from that for conventional solar cells. As shown the carrier transportation of SIS device under lumination in figure 3, the photo-generated electrons in the depletion region are enforced to move to the right then are collected by the back electrodes; however the photo-generated holes in depletion and diffusion region are forced to move to the left and blocked by the SiO_x barrier as the valence band offset is larger than 4 eV for the SiO_2/Si interface [33]. The blocked holes form recombination current through SiO_x/Si interface states or defect states within the ITO band gap after tunnel. Only the photo-generated electrons in depletion region collected by the back electrodes to form the photon-generated current, so the depletion and absorption regions are the same. The I_{ph} can be given:

$$I_{SC} \approx I_{ph} = q\int_0^{W_n} N\alpha e^{-\alpha x}dx = qN(1 - e^{-\alpha W_n}) \tag{11}$$

where N is the number of photons incident on the surface; α is the absorption coefficient of silicon and W_n is the depletion (or absorption) width. The value of qN is 6.53 mA. And the depletion width W_n can be expressed as:

$$W_n(k_0T) = \left[\frac{2\varepsilon V_D(k_0T)}{q}\frac{1}{N_D}\right]^{\frac{1}{2}} \tag{12}$$

where, the ε is the relative permittivity of silicon. Values of V_D (k_0T) can be obtained by equations (4) and (6). As the temperature decreases, V_D is increased, thus leading to W_n increases. At 300 K, W_n is about 0.77 μm. The corresponding calculated value of α is 1.15×10^4 cm^{-1} which is in reasonable ranges.

As c-silicon is an indirect bandgap semiconductor, the electronic transition process is phonon-involved, so α is limited by the number of phonons, with a temperature related expression as [34]:

$$\alpha = B\left[\frac{(h\nu - E_g - E_{phonon})^2}{1 - \exp\left(\frac{-E_{phonon}}{k_0T}\right)} + \frac{(h\nu - E_g + E_{phonon})^2}{\exp\left(\frac{E_{phonon}}{k_0T}\right) - 1}\right] \tag{13}$$

where the ν is light frequency; h is Planck's constant ($h\nu$ is the energy of a photon with frequency ν); e.g. is the band gap energy; B is a certain frequency-independent constant; and E_{phonon} is the energy of phonon, which is about 30 meV of c-silicon [31]. Then equation (13) may be rewritten as:

$$\begin{aligned}\alpha &= \alpha_1 + \frac{\alpha_2}{\exp\left(\frac{E_{phonon}}{k_0T}\right) - 1}\\ \alpha_1 &= B(\hbar\omega - E_g - E_{phonon})^2\\ \alpha_2 &= B[(\hbar\omega - E_g - E_{phonon})^2 + (\hbar\omega - E_g + E_{phonon})^2]\end{aligned} \tag{14}$$

The value of α_1 is more than twice the value of α_2. The I_{SC} may be expressed as:

$$I_{SC} = qN\left[1 - \exp\left(-\left(\alpha_1 + \alpha_2 \Big/ \left(\exp\left(\frac{E_{phonon}}{k_0T}\right) - 1\right)\right) * W_n(k_0T)\right)\right] \tag{15}$$

By fitting the experimental data illustrated in figure 5(c), with the well-derived expression of photon-generated current, we get a good match between the experimental results and the theoretical model, as shown in figure 10. The specific values of those physical parameters for fitting are shown in table 2. The value of α_2 is 1.3×10^{-4} cm^{-1} which is more than twice the value of 0.5×10^{-4} $cm^{-1}$of α_1. Significantly, the quantity E_{phonon} of 28 meV has been obtained even at very low temperature range, which is consistent with the phonon energy in crystal silicon [31]. Hence, the interaction of the 'cold electron or hole' and phonon in the bulk silicon would influence the variation of I_{ph} or I_{SC} with the temperature, probably, the subsidiary materials somewhere like ITO, SiO_x and intermediate emitter layer also plays a role for the carrier transport, because the increase of I_{ph} is fundamentally dependent on the absorption coefficient and depletion width of the silicon substrate and the device.

4. Conclusion

The temperature responses of *I–V* characteristics of ITO/SiO_x/c-Si heterojunction solar cell in the range of 10–300 K

were investigated by using single energy concentrated photons illumination (667 mW cm^{-2}), and it is found that the change of I_{SC} and V_{OC} are much larger than that of *FF* and *Eff*. With the increase of the temperature from 10 to 300 K, I_{SC} increases from 2.26 to 3.84 mA cm^{-2} and V_{OC} decreases from 0.74 to 0.46 V. However, their variation is non-linear. At standard conditions, the SIS device possesses the stable PV properties with the built-in potential of 0.57 V, open-circuit voltage V_{OC} of 0.51 V, short-circuit current density J_{SC} of 24.3 mA cm^{-2}, filled factor *FF* of 71.1% and conversion efficiency of 8.8%, respectively. From the verification of *FF* and R_{sh} by the experimental measurements and the modeling, the carrier recombination at the low temperature (<100 K) is insensitive and rarely influences V_{OC}. The fact is ascribed to the good SiO_x passivation layer at the interface between ITO and c-Si. Thus, the energy band diagram shows that there is an inversion layer in silicon near the ITO/SiO_x/c-Si interface.

Moreover, based on the analyses of diode model and curve fitting of the experimental data, it is found that as the temperature rises, the narrowing of silicon band gap and the shift of Fermi level in silicon is the reason accounting for the drop of V_{OC}; and the increase of I_{SC} results from the widening of depletion width and the increased absorption coefficient in silicon. The effects of the changes of carrier recombination, semiconductor band gap and parasitic resistance on photoelectronic parameters of SIS solar cell are also calculated and discussed at different temperatures, all of which are meaningful for SIS photovoltaic device in low temperature application.

Acknowledgment

This work was partly supported by the National Natural Science Foundation (No. 60876045 and 61306072) of China, Shanghai Leading Basic Research Project (No. 09JC1405900), and R&D Foundation of SHU-SOENs PV Joint Lab (No. SS-E0700601). This appreciation was also given to Instrumental Analysis & Research Center of Shanghai University for their help in microstructure measurements of the samples.

References

[1] Saga T 2010 Advances in crystalline silicon solar cell technology for industrial mass production *NPG Asia Mater.* **2** 96–102
[2] Dobrzański L A, Musztyfaga M and Drygała A 2013 Final manufacturing process of front side metallisation on silicon solar cells using conventional and unconventional techniques, Strojniški vestnik *J. Mech. Eng.* **59** 175–82
[3] Bowden S, Das U, Herasimenka S and Birkmire R 2008 Stability of amorphous/crystalline silicon heterojunctions *33rd Photovoltaic Specialists Conf. (San Diego, CA, USA, 2008)* p 1–4
[4] Wagner L and Grossman J 2008 Microscopic description of light induced defects in amorphous silicon solar cells *Phys. Rev. Lett.* **101** 265501
[5] Bethge O, Nobile M, Abermann S, Glaser M and Bertagnolli E 2013 ALD grown bilayer junction of ZnO : Al and tunnel oxide barrier for SIS solar cell *Sol. Energy Mater. Sol. Cells* **117** 178–82
[6] Du H W, Yang J, Li Y H, Xu F, Xu J and Ma Z Q 2015 Preparation of ITO/SiO_x/n-Si solar cells with non-decline potential field and hole tunneling by magnetron sputtering *Appl. Phys. Lett.* **106** 093508
[7] Kim J, Yun J-H, Park Y C and Anderson W A 2012 Transparent and crystalline Al-doped ZnO film-embedded heterojunction Si solar cell *Mater. Lett.* **75** 99–101
[8] Hamberg I and Granqvist C G 1986 Evaporated Sn-doped In_2O_3 films: basic optical properties and applications to energy-efficient windows *J. Appl. Phys.* **60** R123
[9] Malik O, De la Hidalga-W F J, Zúñiga-I C and Ruiz-T G 2008 Efficient ITO–Si solar cells and power modules fabricated with a low temperature technology: results and perspectives *J. Non-Cryst. Solids* **354** 2472–7
[10] Zhou H, Wei D, Xu S, Xiao S, Xu L, Huang S, Guo Y, Khan S and Xu M 2012 Si surface passivation by SiO_x : H films deposited by a low-frequency ICP for solar cell applications *J. Phys. D: Appl. Phys.* **45** 395401
[11] Dhariwal S, Jain S and Kothari L 1975 Surface recombination and internal currents in a vertical-junction solar cell *J. Phys. D: Appl. Phys.* **8** 1321
[12] Zhong C, Yao R and Geng K 2010 Characterization of interface states in a-Si: H/c-Si heterojunctions by an expression of the theoretical diffusion capacitance *J. Phys. D: Appl. Phys.* **43** 495102
[13] Fang H-W, Hsieh T-E and Juang J-Y 2013 Influences of SiO_x layer thickness on the characteristics of In–Zn–O/SiO_x/n-Si hetero-junction structure solar cells *Surf. Coat. Technol.* **231** 214–8
[14] Fang H-W, Liu S-J, Hsieh T-E, Juang J-Y and Hsieh J-H 2011 Fabrication and characterization of amorphous In–Zn–O/SiO_x/n-Si heterojunction solar cells *Sol. Energy* **85** 2589–94
[15] Cheknane A 2009 Analytical modelling and experimental studies of SIS tunnel solar cells *J. Phys. D: Appl. Phys.* **42** 115302
[16] Tayagaki T, Hoshi Y and Usami N 2013 Investigation of the open-circuit voltage in solar cells doped with quantum dots *Sci. Rep.* **3** 2703
[17] Yoon S and Garboushian V 1994 Reduced temperature dependence of high-concentration photovoltaic solar cell open-circuit voltage (V_{OC}) at high concentration levels *24th IEEE Photovoltaic Specialists Conf.* (*Waikoloa, HI, 1994*) (doi: 10.1109/WCPEC.1994.520235)
[18] Al-Naser Q A H, Al-barghoothi N M A and Al-Ali N A S 2012 The effect of temperature variations on solar cell efficiency *Int. J. Eng.* **13–134** 108–12
[19] Mizrah T and Adler D 1976 Operation of ITO/Si heterojunction solar cells *Appl. Phys. Lett.* **29** 682
[20] Schulze T F, Korte L, Conrad E, Schmidt M and Rech B 2010 Electrical transport mechanisms in a-SiH/c-Si heterojunction solar cells *J. Appl. Phys.* **107** 023711
[21] Scheer R 2009 Activation energy of heterojunction diode currents in the limit of interface recombination *J. Appl. Phys.* **105** 104505
[22] Logofatu C, Negrila C C, Ghita R V, Ungureanu F, Cotirlan C, Manea C G A S and Lazarescu M F 2011 Study of SiO_2/Si interface by surface techniques *Crystalline Silicon—Properties and Uses* ed S Basu (Croatia: InTech) pp 23–42 (http://cdn.intechopen.com/pdfs-wm/17722.pdf)
[23] Lu Z H, McCaffrey J P, Brar B, Wilk G D, Wallace R M, Feldman L C and Tay S P 1997 SiO_2 film thickness metrology by x-ray photoelectron spectroscopy *Appl. Phys. Lett.* **71** 2764
[24] Ghannam M, Shehadah G, Abdulraheem Y and Poortmans J 2015 On the possible role of the interfacial inversion layer in the improvement of the performance of hydrogenated amorphous silicon/crystalline silicon heterojunction solar cells [HIT] *Sol. Energy Mater. Sol. Cells* **132** 320–8
[25] Madani Ghahfarokhi O, von Maydell K and Agert C 2014 Enhanced passivation at amorphous/crystalline silicon interface and suppressed Schottky barrier by deposition

of microcrystalline silicon emitter layer in silicon heterojunction solar cells *Appl. Phys. Lett.* **104** 113901
[26] Hegedus S S and Shafarman W N 2004 Thin-film solar cells: device measurements and analysis *Prog. Photovol.: Res. Appl.* **12** 155–76
[27] Thakur A K, Wantz G, Garcia-Belmonte G, Bisquert J and Hirsch L 2011 Temperature dependence of open-circuit voltage and recombination processes in polymer-fullerene based solar cells *Sol. Energy Mater. Sol. Cells* **95** 2131–5
[28] Liang J, Schiff E A, Guha S, Yan B and Yang J 2005 Temperature-dependent open-circuit voltage measurements and light-soaking in hydrogenated amorphous silcon solar cells *Mater. Res. Soc. Symp. Proc.* **862** A21.28.21–6 (http://surface.syr.edu/cgi/viewcontent.cgi?article=1042&context=phy)
[29] Usami A, Seki S, Mita Y, Kobayashi H, Miyashiro H and Terada N 2009 Temperature dependence of open-circuit voltage in dye-sensitized solar cells *Sol. Energy Mater. Sol. Cells* **93** 840–2
[30] Huang K M, Wang K L, Wang D P, Huang K F, Huang T C and Chu A K 1997 Temperature dependence of Fermi level obtained by electroreflectance spectroscopy of undoped n_+-type doped GaAs *Appl. Phys. Lett.* **71** 3889
[31] O'Donnell K P and Chen X 1991 Temperature dependence of semiconductor band gaps *Appl. Phys. Lett.* **58** 2924–6
[32] Sze S M and Ng K K 2006 *Physics of Semiconductor Devices* (Hoboken, NJ: Wiley) p 5–75
[33] Liebhaber M, Mews M, Schulze T F, Korte L, Rech B and Lips K 2015 Valence band offset in heterojunctions between crystalline silicon and amorphous silicon (sub)oxides (a-SiO_x : H, $0 < x < 2$) *Appl. Phys. Lett.* **106** 031601
[34] Pankove J I 2012 *Optical Processes in Semiconductors* (New York: Dover)